Stem Cell Research & Therapy

RESEARCH

Open Access

Mesenchymal cell-derived exosomes and miR-29a-3p mitigate renal fibrosis and vascular rarefaction after renal ischemia reperfusion injury

Jing Huang[1], Lang Shi[4], Yifei Yang[1], Fan Zhao[1], Rengui Chen[1], Wenliang Liao[1], Jiefu Zhu[2], Dingping Yang[1*], Xiongfei Wu[3*] and Shangting Han[2*]

Abstract

Background Renal fibrosis and vascular rarefaction are significant complications of ischemia/reperfusion (I/R) injury. Human umbilical cord mesenchymal cell-derived exosomes (hucMSC-exos) have shown potential in mitigating these conditions. This study investigates the role of miR-29a-3p in exosomes and its therapeutic effects on I/R-induced renal damage.

Methods Male C57BL/6 mice were subjected to unilateral renal ischemia for 28 min followed by reperfusion. Exosomes and miR-29a-3p mimics/inhibitors were injected into the mice. Renal function, histological analysis, and molecular assays were performed to evaluate fibrosis and vascular integrity.

Results Exosome treatment significantly improved renal function and reduced fibrosis and vascular rarefaction post-I/R. MiR-29a-3p was highly expressed in hucMSC-exos but reduced in renal fibrosis models. MiR-29a-3p mimic reduced, while its inhibitor exacerbated I/R-induced renal fibrosis and vascular rarefaction. Collagen I and TNFR1 were identified as direct targets of miR-29a-3p in fibroblasts and endothelial cells, respectively. Exosomes overexpressing miR-29a-3p provided superior protection compared to unmodified hucMSC-exos.

Conclusion HucMSC-exos, particularly those overexpressing miR-29a-3p, have potent therapeutic effects against renal fibrosis and vascular rarefaction post-I/R. MiR-29a-3p targets TNFR1 and collagen I, highlighting its potential in renal fibrosis therapy.

Keywords Mesenchymal stem cell exosomes, Renal ischemia reperfusion injury, Renal fibrosis, Vascular rarefaction, microRNA

*Correspondence:
Dingping Yang
shenbinneike@163.com
Xiongfei Wu
wuxfei@126.com
Shangting Han
2019283020148@whu.edu.cn
Full list of author information is available at the end of the article

Backgound

The development and progression of tubulointerstitial fibrosis (TIF) constitute a complex process involving a myriad of distinct cell types. Multiple cellular components contribute to the advancement of TIF, including renal tubular epithelial cells, myofibroblasts, endothelial cells, and inflammatory cells [1–4]. Upon activation, fibroblasts transform into myofibroblasts expressing α-smooth muscle actin (α-SMA), subsequently generating ECM components such as collagen-1a1 (COL1A1) and fibronectin (FN) [5, 6]. These processes directly contribute to the initiation and progression of renal fibrosis. Moreover, endothelial cell injury, resulting from inflammation and hypoxia, leads to endothelial collapse, capillary rarefaction, and impaired blood supply, further exacerbating renal fibrosis [7–11]. Despite the significant advancements in understanding the mechanisms of renal fibrosis in recent years, there are still no effective drugs available for its treatment [12].

Over the past decade, a promising trend has emerged in utilizing various types of mesenchymal stem cells (MSCs) to address organ fibrosis [13, 14]. A key mechanism in MSC-based therapies is the paracrine activity of secreted factors, often mediated by extracellular vesicles (EVs). Exosomes, a subtype of EVs, are potent cell-to-cell communicators within the MSC secretome, known for their low immunogenicity and tumorigenicity. Notably, exosomes released by hucMSCs have shown significant potential in improving tissue regeneration [15]. This improvement is largely attributed to small EVs (40–150 nm) carrying regulatory microRNAs (miRNAs), which are pivotal mediators of their therapeutic effects [16]. Among these miRNAs, miR-29a-3p has emerged as a key regulator of fibrosis in various organs, including the kidney [16, 17]. It has been implicated in suppressing extracellular matrix production and modulating inflammatory responses [16]. However, the specific role of miR-29a-3p and MSC-derived exosomes in the context of renal I/R injury remains to be fully elucidated.

This study aims to investigate the therapeutic potential of MSC-derived exosomes, particularly those enriched with miR-29a-3p, in mitigating renal fibrosis and vascular rarefaction following I/R injury. We hypothesize that miR-29a-3p-enriched exosomes will exert superior protective effects compared to regular exosomes by targeting key molecular pathways involved in fibrosis and vascular damage. Through comprehensive in vivo and in vitro analyses, we seek to delineate the mechanisms by which miR-29a-3p and hucMSC-exos modulate renal fibrosis and vascular integrity, thereby providing insights into potential therapeutic strategies for renal fibrosis.

Method

Cell culture and intervention methods

Human Umbilical Vein Endothelial Cells (HUVECs) were obtained from the China Centre for Type Culture Collection, which confirmed ethical approval and informed consent from donors (http://cctcc.whu.edu.cn/). Normal Rat Kidney Fibroblast Cells (NRK-49F) were obtained from the Shanghai Institute for Biological Sciences. HUVECs were cultured in DMEM/F12 medium (Hyclone), while NRK-49F cells were cultured in high-glucose Dulbecco's Modified Eagle's Medium (DMEM, Hyclone). Both media were supplemented with 1% penicillin–streptomycin and 10% fetal bovine serum, and the cells were incubated at 37 °C in a humidified atmosphere with 5% CO_2. HUVECs and NRK-49F cells were seeded at a density of 0.3×10^6 cells per 35 mm dish. HUVECs were treated with 20 ng/mL TNFα (R&D, 210-TA), while NRK-49F cells were treated with 10 ng/mL TGF-β.

In some experiments, HUVECs and NRK-49F cells were transfected with lentivirus-packaged miR-29a-3p mimics or corresponding negative controls (NC). The lentiviral vectors were obtained from GenePharma. The Mimics group was transfected with lentivirus-packaged miR-29a-3p mimics, while the NC group was transfected with an empty lentivirus. The multiplicity of infection (MOI) for both groups was 20, with 5 μg/ml Polybrene added to the medium. After 16 h of transfection, the medium containing lentivirus was replaced with fresh medium. Transfection efficiency was assessed 48 h later using an inverted fluorescence microscope. The work has been reported in line with the ARRIVE guidelines 2.0.

HucMSC-exos isolation and purification

HucMSCs, donated by Hamilton Biology (Wuhan, China), were cultured in mesenchymal stem cell medium (ScienCell, USA) at 37°C in a humidified atmosphere containing 5% CO_2. For MSC-exos preparation, hucMSCs (passages 2–6) were cultured in serum-free stem cell culture medium for 48 h, and the supernatant was collected for MSC-exos extraction. MSC-exos were isolated through gradient centrifugation and filtration. Briefly, the supernatant was centrifuged at 2000×g for 20 min, then at 13,500×g for 30 min, filtered through a 0.22 μm filter, and ultracentrifuged at 200,000×g for 120 min at 4 °C (Beckman Coulter Optima L-80 XP). The exosome pellet was resuspended in sterile phosphate-buffered saline (PBS), filtered again through a 0.22 μm membrane filter for purity, and stored at − 80 °C.

HucMSC-exos identification

The morphology of hucMSC-exos was observed using transmission electron microscopy (TEM). Briefly, exosomes were fixed in 2% paraformaldehyde and loaded

onto a carbon-coated copper grid. After drying for 20 min at room temperature, grids were stained with 2% uranyl acetate. Western blotting was used to detect cell surface markers, including exosome markers (Alix, CD63, Tsg101, CD9), and negative controls, such as Golgi markers (GM130).

Animal model and intervention methods

Male C57 BL/6J mice were purchased and housed at the Center of Experimental Animals at Wuhan University. All animal protocols were approved by the Animal Care and Use Committee of Renmin Hospital of Wuhan University. Prior to experimental procedures, mice were anesthetized with Pentobarbital Sodium administered intraperitoneally at a dose of 50 mg/kg to induce deep anesthesia. Additionally, Buprenorphine was administered at a dose of 0.1 mg/kg to alleviate pain. Mice were subjected to 28 min of left renal pedicle clamping to induce I/R injury, as previously described [18]. The body temperature of the mice was monitored and maintained at ~36.5 °C using a homeothermic blanket control unit with sensitive rectal probe. Sham-operated mice underwent kidney exposure without clamping. The sample size was estimated based on our previous publication without conducting a prior power analysis. No inclusion or exclusion criteria were defined, and no animals were excluded from the analysis. All mice were sacrificed 14 days post-surgery, and the right kidney was removed 24 h before sacrifice to observe renal function changes. In this study, randomization was used to allocate experimental units to control and treatment groups. The randomization sequence was generated using a random number generator. Humane endpoints were established to ensure animal welfare, including significant weight loss (>30%), behavioral changes (such as reduced activity), and signs of pain or discomfort.

To study the effect of hucMSC exosomes on I/R-induced renal fibrosis, the hucMSC exosomes treatment group received 50 μg of hucMSC exosomes via tail vein injection at −1 d, 0, 3 d, 6 d, and 9 d post-reperfusion, while the control group received an equal volume of vehicle. To investigate the impact of miR-29a-3p on I/R-induced renal fibrosis, mice were randomly divided and injected with NC lentivirus, miR-29a-3p mimics lentivirus, or miR-29a-3p Inhibitor lentivirus into the left renal cortex 10 days before I/R, as previously described [19]. All animals are kept in the same environment conditions, such as temperature, humidity, and light/dark cycles to minimize variability. At the end of the experiment, mice were euthanized humanely using CO_2 inhalation in a chamber followed by cervical dislocation to ensure death. We implemented blinding procedures so that the researchers conducting the measurements were unaware of the treatment groups, minimizing observer bias.

Patients

Kidney biopsy specimens were collected from CKD patients undergoing diagnostic evaluation in the Department of Nephrology at Renmin Hospital of Wuhan University. The control group included kidney samples from the adjacent non-cancerous tissues of renal cancer patients. Detailed patient information is shown in Table 1.

Histopathology staining

Kidneys were fixed in 4% paraformaldehyde at room temperature and embedded in paraffin. Sections were stained with HE and Masson trichrome to observe pathological changes. Tubular injury was defined by the presence of cell lysis, loss of brush border, and cast formation. Tubular injury was scored by the percentage of damaged tubules: 0, no damage; 1, <25%; 2, 25–50%; 3, 50–75%; 4, >75%. Ten random fields per mouse kidney were scored for quantification, and the average value was used as the tubular injury score. Collagen volume fraction was calculated using Image J by measuring the percentage of the blue-stained area (collagen) in each field. Ten random fields per mouse kidney were selected at 200× magnification for quantification.

Western blotting

Immunoblotting was performed using standard methods as previously described [20].Total protein was extracted using RIPA buffer (Thermo Fisher Scientific, USA) containing protease inhibitors. Proteins were separated by

Table 1 Clinical data of CKD and non-CKD patients examined

Parameter	CKD (n = 10)	Control (n = 10)	*P* value
Clinical indexes			
sex	M (8) F (2)	M (5) F (5)	
Age (year)	46.6 ± 13.00	47.6 ± 12.55	0.870
Hypertension	100%	30%	
Diabetes	20%	10%	
Diagnosis	CKD (10)	Para-cancer renal tissue (10)	
Fibrosis	48 ± 13.3*	3 ± 1.71	< 0.001
Global sclerosis	56 ± 10.9*	12 ± 6.93	< 0.001
Laboratory data			
BUN (mmol/L)*	8.2 ± 0.85*	5.42 ± 0.89	< 0.001
Scr (mmol/L)*	181.3 ± 42.75*	72.6 ± 8.90	< 0.001
ALB (G/L)	37.44 ± 2.83	40.35 ± 2.53	0.03
UTP (G/24H)	1.91 ± 0.60*	0.28 ± 0.11	< 0.001

(2-tailed student's t-test for comparison). *Statistically significant difference between DKD and non-DKD group

SDS-PAGE, transferred to PVDF membranes (Millipore, USA). The PVDF membranes were incubated overnight at 4℃ with primary antibodies against COL1A1 (Novus Biologicals, NBP1-30054; 1:500), FN1 (Abcam, ab2413; 1:2000), ACTA2/α-SMA (Abcam, ab5694; 1:1000), TNFα (Santa Cruz, sc-8436; 1:250), ICAM-1 (Santa Cruz, sc-8439; 1:400), VCAM-1 (Abcam, ab13047; 1:2000), GAPDH (Proteintech, 60004–1-lg; 1:5000), CD9 (abcam, ab92726; 1:1000), TSG101 (Santacruz, Sc-7964; 1:800), CD63 (Santacruz, Sc-5275; 1:800), ALIX (Santacruz, Sc-53540; 1:800), IL-1β (Santacruz, Sc-52012; 1:1000), GM130 (Cell Signaling Technology, 12480; 1:1000). The PVDF membranes were incubated with the secondary antibody at room temperature for 1 h. The signal was then detected using an ECL kit (Thermo Fisher Scientific, USA) and quantified using ImageJ software.

Real-time quantitative polymerase chain reaction (RT-PCR)

Total RNA was extracted from cultured cells and tissue samples using TRIzol reagent (Invitrogen, USA) following the manufacture's instructions. RNA quality and concentration was determined with NanoDrop 2000 specrophotometer (Thermo Scientific, USA). cDNA synthesis was performed using a reverse transcription kit (Thermo Fisher Scientific, USA). Target gene mRNA expression levels were measured using a real-time quantitative PCR system (Bio-Rad, USA). Primers for miR-29a-3p were designed and synthesized by Sangon Biotech (Sangon Biotech). Procedures were performed according to the manufacturer's instructions. Relative expression levels of target genes were calculated using the 2^(−ΔΔCt) method. All reactions were performed in triplicate to ensure reproducibility.

Immunofluorescence analysis

Immunofluorescence assays were performed as previously described [21]. Cultured cells were permeabilized with 0.1% Triton X-100 for 30 min and blocked with 5% bovine serum albumin (BSA) for 1 h at room temperature. Primary antibodies for immunohistochemical staining included FN1 (Abcam, ab2413; 1:200), ACTA2/α-SMA (Abcam, ab5694; 1:200), CD31 (Abcam, ab28364; 1:50). Primary antibodies incubated with the cells overnight at 4°C. After washing with phosphate-buffered saline (PBS), the samples were incubated with fluorescently labeled secondary antibodies, including Cy3-conjugated goat anti-mouse IgG and FITC-conjugated goat anti-rabbit IgG (both from Jackson lmmunoResearch), for 1 h at room temperature. Nuclei were counterstained with DAPI (4',6-diamidino-2-phenylindole, Sigma-Aldrich, USA). Positive staining areas were quantified using Image-ProPlus 6.0 software. Semi-quantitative histological and immunohistochemical staining was independently performed by two blinded pathologists to ensure consistency.

Luciferase reporter assay

NRK-49F cells were co-transfected with 3′UTR luciferase reporter constructs (3′UTR-NC, 3′UTR-COL1A1-wt, 3′UTR-COL1A1-mutant), miRNA (miRNA-NC or miR-29a-3p), and Renilla luciferase using GP-transfect-Mate (GenePharma, China). Similarly, endothelial cells were co-transfected with 3′UTR luciferase reporter constructs (3′UTR-NC, 3′UTR-TNFR1-wt, 3′UTR-TNFR1-mutant), miRNA (miRNA-NC or miR-29a-3p), and Renilla luciferase using GP-transfect-Mate (GenePharma). After 48 h of transfection, luciferase activity was measured using a dual-luciferase reporter assay kit (Promega, USA) following the manufacturer's protocol. Luminescence was detected on a Tecan Infinite M1000 microplate reader.

Statistical analysis

All data represent at least three independent experiments and were analyzed using GraphPad Prism 9. Data were expressed as mean ± SD. A t-test was employed to determine significant differences between two groups. One-way or two-way ANOVA was used with multiple

(See figure on next page.)

Fig. 1 Exosomes intervention reduces TGF-β-induced fibroblast activation and TNF-α-induced endothelial cell injury. **A** Representative electron microscopy image of isolated exosomes. **B** Western blot analysis of exosome markers CD9, Tsg101, CD63, Alix, and the Golgi marker GM130. **C** Immunofluorescence staining of α-SMA and collagen I in fibroblast cells treated with vehicle (negative control, NC), TGF-β, low and high concentrations of exosomes. Nuclei are stained with DAPI. Scale bars: 20 μm. Quantification of α-SMA-positive signal and collagen I expression are shown as bar graphs. Data are presented as mean ± SD (n = 6). #$p < 0.05$ vs. TGF-β + NC. **D** Western blot analysis of COL1A1, α-SMA, and GAPDH in cells treated with TGF-β and exosomes. Densitometric analysis of Western blot bands normalized to GAPDH are shown as bar graphs. Data are presented as mean ± SD (n = 6). *$p < 0.05$ vs. Ctrl, #$p < 0.05$ vs. TGF-β + NC. **E** Immunofluorescence staining for ICAM-1 in endothelial cells treated with vehicle, TNF-α, and low or high concentrations of exosomes. Scale bar = 20 μm. Quantification of the area of ICAM-1-positive signal is shown on the right (mean ± SD, #$p < 0.05$ vs. TNF-α + NC). **F** Western blot analysis of ICAM-1, VCAM-1, and GAPDH in cells treated with TNF-α and exosomes. Quantification of the relative intensity of VCAM-1 and ICAM-1 signals are shown as bar graphs. Data are presented as mean ± SD (n = 6). *$p < 0.05$ vs. Ctrl, #$p < 0.05$ vs. TNF-α + NC

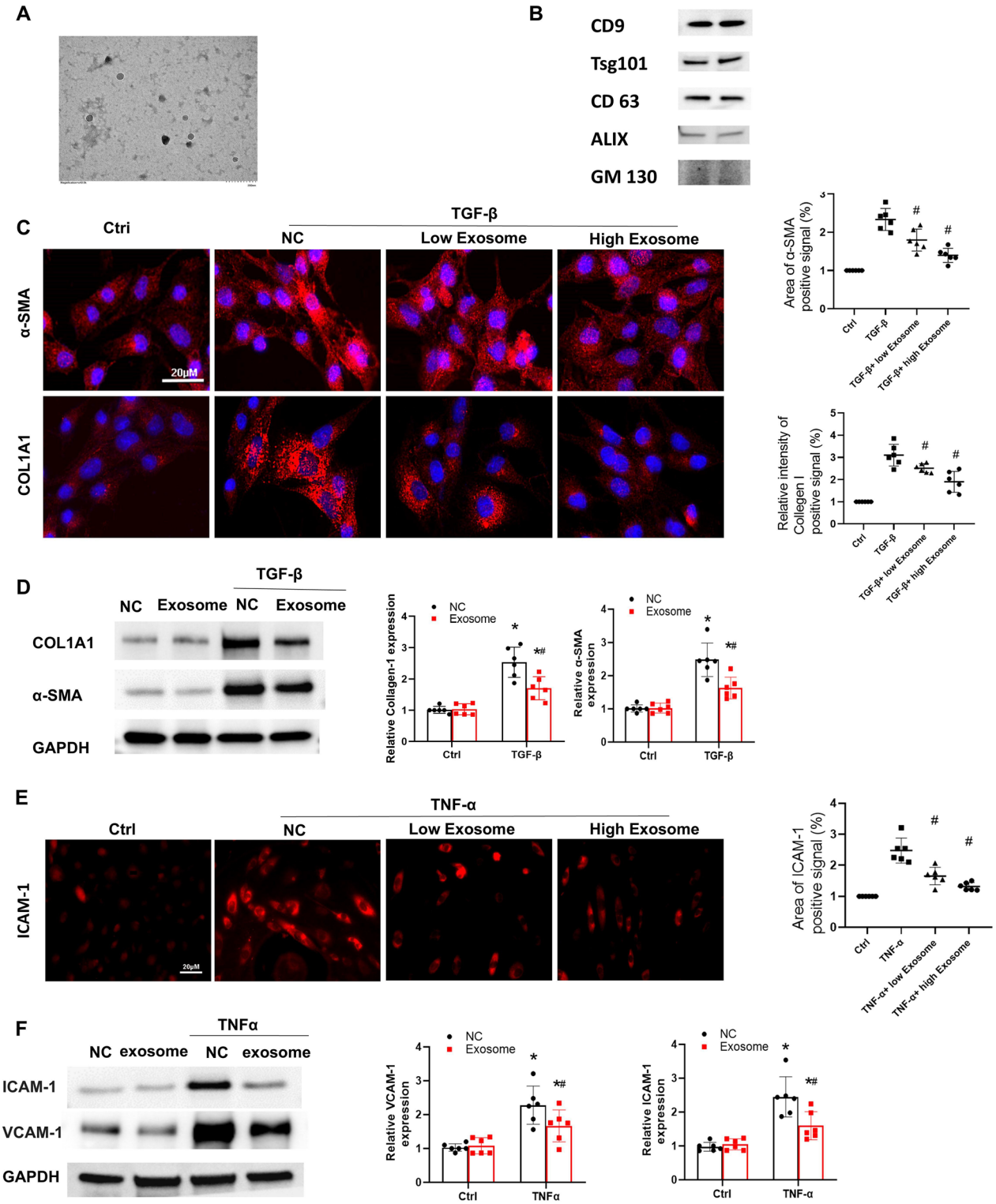

Fig. 1 (See legend on previous page.)

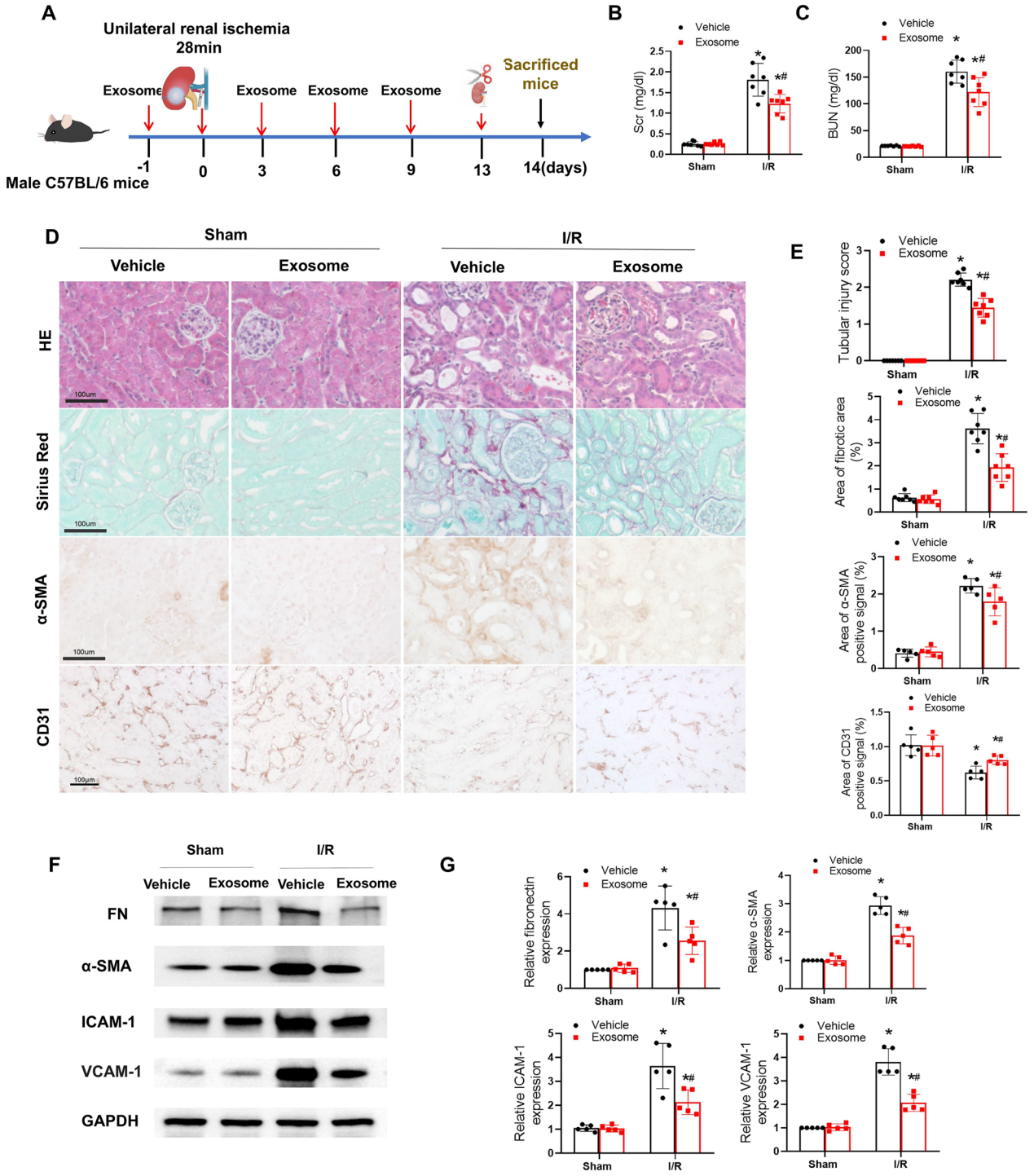

Fig. 2 Mesenchymal Cell-derived Exosomes Improve Renal Fibrosis and Vascular Rarefaction After I/R **A** Schematic diagram of the experimental design. Male C57BL/6 mice underwent 30 min of bilateral renal ischemia followed by reperfusion. Exosomes were administered intravenously at the indicated time points (− 1, 0, 3, 6, 9 days). Mice were sacrificed at 14 days post-I/R injury for analysis. **B** Serum creatinine (Scr) levels and **C** Blood urea nitrogen (BUN) levels were measured to assess renal function. Data are presented as mean ± SD (n = 6). *$p < 0.05$ vs. Sham + Vehicle, #$p < 0.05$ vs. I/R + Vehicle. **D** Representative images of kidney sections stained with Hematoxylin and Eosin (HE), Sirius Red, α-SMA, and CD31. Scale bars: 100 μm. **E** Quantification of tubular injury scores based on HE staining, area of fibrosis based on Sirius Red staining, area of α-SMA positive staining, and area of CD31 positive staining. Data are presented as mean ± SD (n = 5–7). *$p < 0.05$ vs. Sham + Vehicle, #$p < 0.05$ vs. I/R + Vehicle. **F** Western blot analysis of fibronectin (FN), α-SMA, ICAM-1, VCAM-1, and GAPDH in kidney tissues from different groups. **G** Densitometric analysis of Western blot bands normalized to GAPDH. Data are presented as mean ± SD (n = 6). *$p < 0.05$ vs. Sham + Vehicle, #$p < 0.05$ vs. I/R + Vehicle

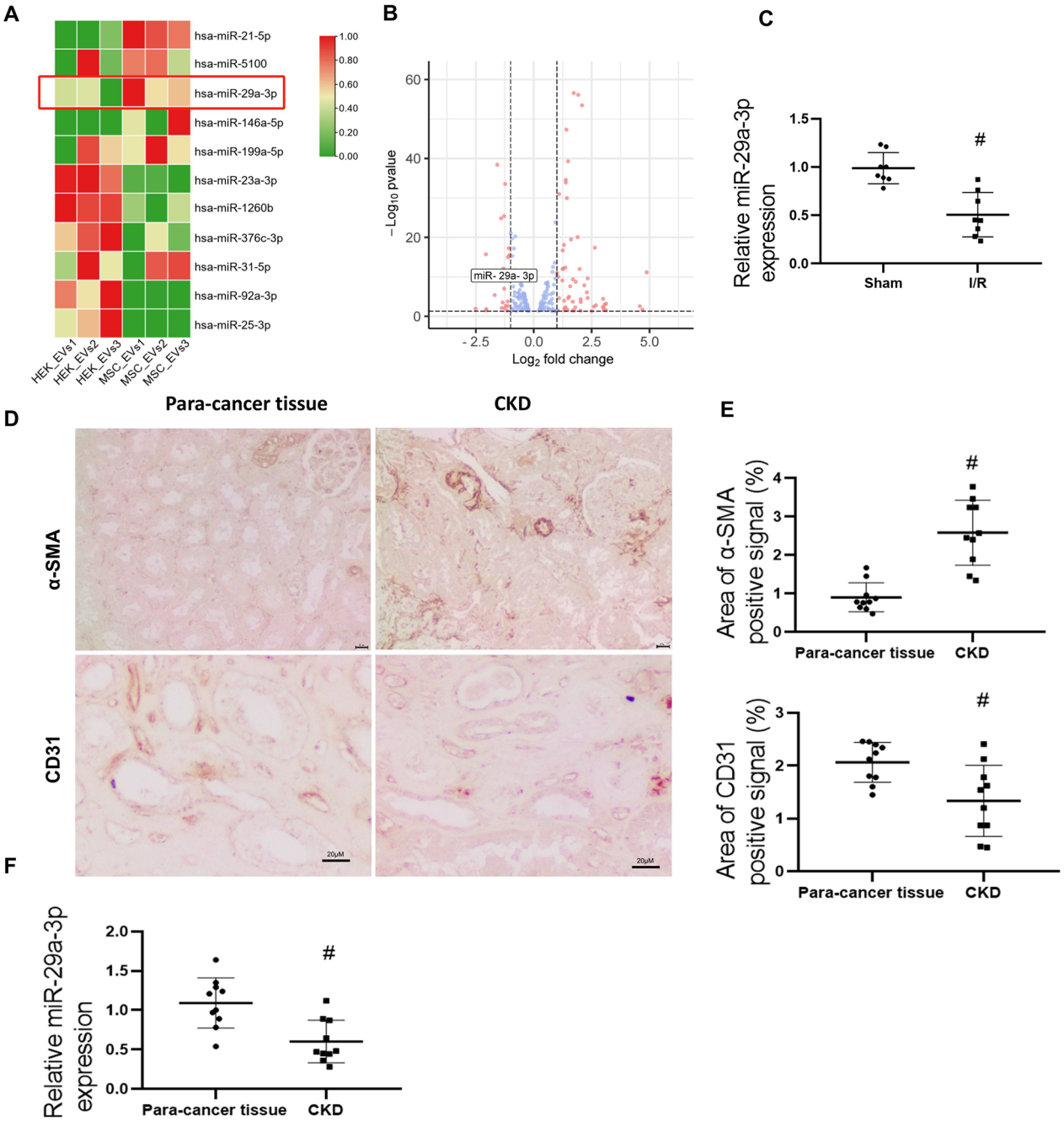

Fig. 3 miR-29a-3p is Highly Expressed in Mesenchymal Cell-derived Exosomes and Reduced in Renal Fibrosis Models **A** Heatmap showing the expression levels of various miRNAs in mesenchymal cell-derived exosomes compared to HEK293-derived exosomes, highlighting the high expression of miR-29a-3p. **B** Volcano plot displaying differentially expressed miRNAs in I/R-induced mouse renal fibrosis models compared to controls, indicating a significant reduction in miR-29a-3p expression in fibrosis models. **C** Quantification of relative miR-29a-3p expression in Sham and I/R groups. Data are presented as mean ± SD (n = 8). #$p < 0.05$ vs. Sham. **D** Representative images of kidney sections stained with α-SMA and CD31 in para-cancer tissue and chronic kidney disease (CKD) tissue. Scale bars: 50 μm. **E** Quantification of the area of α-SMA and CD31 positive signals in para-cancer tissue and CKD tissue. Data are presented as mean ± SD (n = 10). #$p < 0.05$ vs. Para-cancer tissue. **F** Quantification of relative miR-29a-3p expression in para-cancer tissue and CKD tissue. Data are presented as mean ± SD (n = 10). #$p < 0.05$ vs. Para-cancer tissue

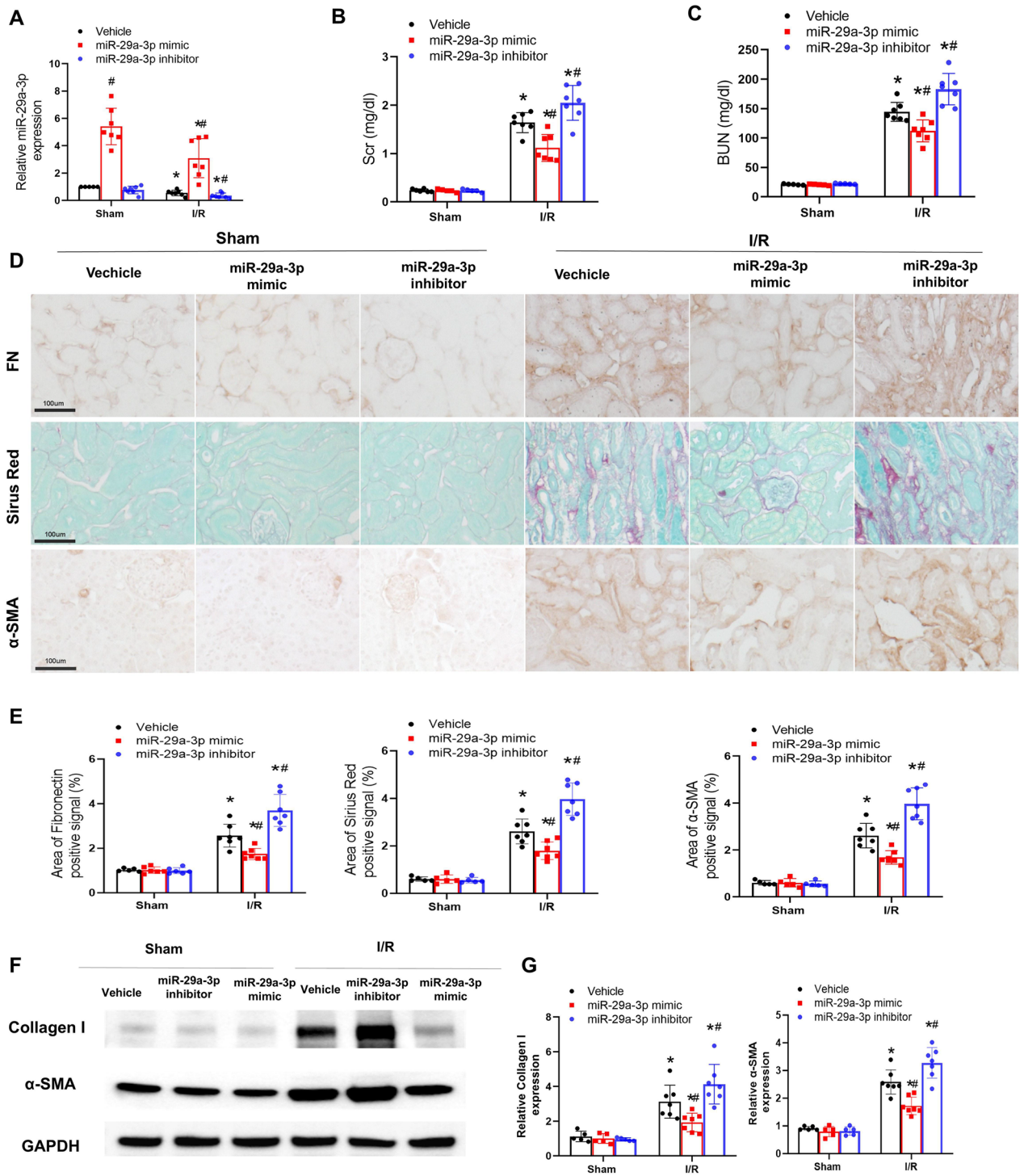

Fig. 4 miR-29a-3p mimic reduces renal fibrosis following ischemia–reperfusion (I/R) njury, while miR-29a-3p inhibitor exacerbates fibrosis. **A** Relative expression levels of miR-29a-3p in sham and I/R groups treated with vehicle, miR-29a-3p mimic, and miR-29a-3p inhibitor. **B** Serum creatinine (Scr) levels in sham and I/R groups treated with vehicle, miR-29a-3p mimic, and miR-29a-3p inhibitor. **C** Blood urea nitrogen (BUN) levels in sham and I/R groups treated with vehicle, miR-29a-3p mimic, and miR-29a-3p inhibitor. **D** Representative images of kidney sections stained for fibronectin (FN), Sirius Red, and α-SMA in sham and I/R groups treated with vehicle, miR-29a-3p mimic, and miR-29a-3p inhibitor. Scale bars: 100 μm. **E** Quantification of FN-positive signal, fibrotic area and α-SMA-positive signal in kidney sections. **F** Western blot analysis of collagen I, α-SMA, and GAPDH in kidney tissues from sham and I/R groups treated with vehicle, miR-29a-3p mimic, and miR-29a-3p inhibitor. **G** Quantification of relative collagen I and α-SMA expression from Western blot data. Data are presented as mean ± SD (n = 6). *$p < 0.05$ vs. Sham + Vehicle; #$p < 0.05$ vs. I/R + Vehicle

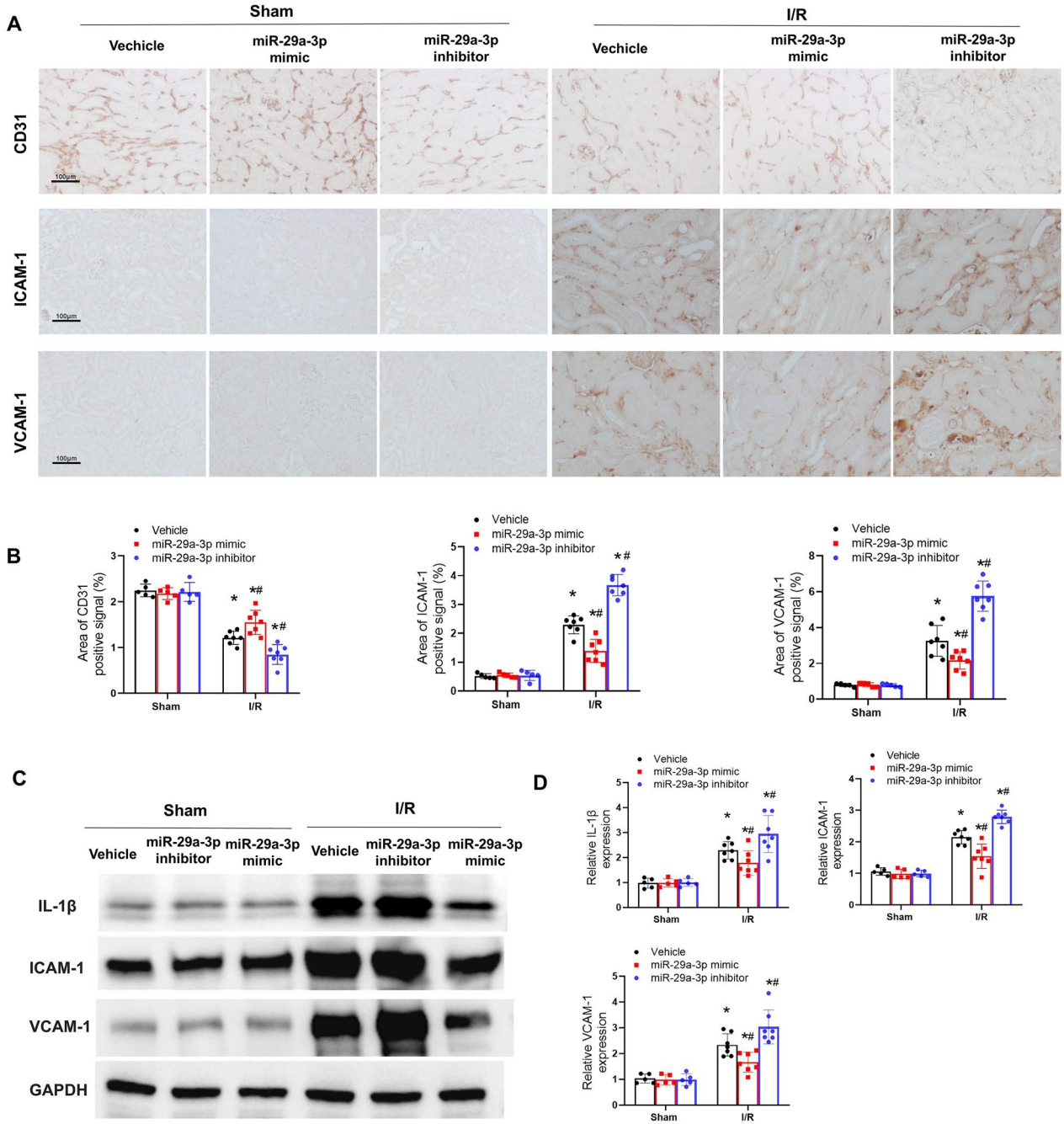

Fig. 5 miR-29a-3p Mimic Reduces, While miR-29a-3p Inhibitor Exacerbates Vascular Rarefaction Caused by I/R in Mice **A** Representative images of kidney sections stained with CD31 in Sham and I/R groups treated with Vehicle, miR-29a-3p inhibitor, or miR-29a-3p mimics. **B** Quantification of the area of CD31-positive signal, ICAM-1-positive signal, and VCAM-1-positive signal in Sham and I/R groups. Data are presented as mean ± SD (n = 7). *$p < 0.05$ vs. Sham + Vehicle, #$p < 0.05$ vs. I/R + Vehicle. **C** Western blot analysis of IL-1β, ICAM-1, VCAM-1, and GAPDH in kidney tissues from Sham and I/R groups. **D** Densitometric analysis of Western blot bands normalized to GAPDH, showing relative expression levels of IL-1β, ICAM-1, and VCAM-1. Data are presented as mean ± SD (n = 6). *$p < 0.05$ vs. Sham + Vehicle, #$p < 0.05$ vs. I/R + Vehicle

(See figure on next page.)

Fig. 6 Collagen-1 is a Target of miR-29a-3p in Fibroblasts **A** Venn diagram showing the overlap of predicted targets of miR-29a-3p identified by Targetscan, miRDB, and microT-CDS databases. **B** Sequence alignment of miR-29a-3p with the 3′UTR of COL1A1 mRNA, highlighting the target binding site. **C** Sequence of the wild-type (WT) and mutant (Mut) COL1A1 3′UTR used in luciferase reporter assays. **D** Luciferase activity assay showing the relative luciferase activity in cells transfected with WT or Mut COL1A1 3′UTR constructs and miR-29a-3p mimics. Data are presented as mean ± SD (n = 4). #$p < 0.05$ vs. WT COL1A1 3′UTR + NC. **E** Western blot analysis of COL1A1 and GAPDH in fibroblasts transfected with NC or miR-29a-3p mimics. **F** Quantification of COL1A1 protein expression normalized to GAPDH. Data are presented as mean ± SD (n = 6). *$p < 0.05$ vs. NC. **G** Representative immunofluorescence images of fibroblasts treated with vehicle or TGF-β and transfected with NC or miR-29a-3p mimics, stained for α-SMA and collagen I. Scale bars: 20 μm. **H** Quantification of the relative intensity of α-SMA and collagen I positive staining in fibroblasts. Data are presented as mean ± SD (n = 5). *$p < 0.05$ vs. Vehicle + NC mimic, #$p < 0.05$ vs. TGF-β + NC mimic. **I** Western blot analysis of fibronectin (FN), collagen I (COL1A1), α-SMA, and GAPDH in fibroblasts treated with vehicle or TGF-β and transfected with NC or miR-29a-3p mimics. **J** Quantification of α-SMA and collagen I protein expression normalized to GAPDH. Data are presented as mean ± SD (n = 6). *$p < 0.05$ vs. Vehicle + NC mimic, #$p < 0.05$ vs. TGF-β + NC mimic

comparisons. A p-value of less than 0.05 was considered statistically significant.

Result

Mesenchymal cell-derived exosomes reduce TGF-β-induced fibroblast activation and decrease TNF-α-induced endothelial cell injury

To investigate the potential therapeutic effects of mesenchymal cell-derived exosomes on fibroblast activation and endothelial cell injury, we treated fibroblasts with TGF-β and endothelial cells with TNF-α, with and without exosome intervention. Transmission electron microscopy confirmed the successful isolation of exosomes (Fig. 1A). Western blot analysis verified the presence of exosome markers CD9, Tsg101, CD63, and ALIX, and the absence of the negative control marker GM130 (Fig. 1B). Immunofluorescence analysis revealed that exosome treatment significantly reduced α-SMA and collagen I expression in fibroblasts treated with TGF-β (Fig. 1C). Western blot analysis corroborated these findings, showing reduced levels of collagen I and α-SMA in exosome-treated fibroblasts (Fig. 1D). In endothelial cells, exosomes decreased TNF-α-induced expression of ICAM-1 and VCAM-1 (Fig. 1E, F). These results indicate that mesenchymal cell-derived exosomes mitigate fibroblast activation and endothelial cell injury induced by TGF-β and TNF-α, respectively.

Mesenchymal cell-derived exosomes improve renal fibrosis and vascular rarefaction after I/R

Given the promising results observed in vitro, we next assessed the effects of mesenchymal cell-derived exosomes on renal fibrosis and vascular rarefaction following ischemia/reperfusion (I/R) injury in mice. Exosome treatment significantly improved renal function, as indicated by lower serum creatinine (Scr) and blood urea nitrogen (BUN) levels compared to the vehicle group (Fig. 2B, C). Histological analysis showed reduced tubular injury scores, fibrosis (Sirius Red staining), and α-SMA positive areas in exosome-treated mice (Fig. 2D, E). Western blot analysis demonstrated decreased expression of fibronectin (FN), α-SMA, ICAM-1, and VCAM-1 in the exosome-treated group (Fig. 2F, G). These findings suggest that hucMSC-exos have a protective effect against renal fibrosis and vascular rarefaction post-I/R.

miR-29a-3p is highly expressed in mesenchymal cell-derived exosomes and reduced in renal fibrosis models

To further explore the molecular mechanisms underlying the therapeutic effects of mesenchymal cell-derived exosomes, we focused on the role of miR-29a-3p. Heatmap analysis revealed high expression of miR-29a-3p in mesenchymal cell-derived exosomes (Fig. 3A). Conversely, miR-29a-3p expression was significantly reduced in both mice post-ischemic fibrosis models and human chronic renal fibrosis samples (Fig. 3B, C, F). Immunohistochemical analysis showed increased α-SMA and decreased CD31 positive signals in chronic kidney disease (CKD) tissues compared to para-cancer tissues, confirming the fibrotic phenotype (Fig. 3D, E). Further experimental results indicated that the relative expression level of miR-29a-3p was significantly reduced in CKD tissues compared to para-cancer tissues (Fig. 3F and Table 1). These results suggest that miR-29a-3p may play a critical role in renal fibrosis.

miR-29a-3p mimic reduces renal fibrosis caused by I/R in mice, while miR-29a-3p inhibitor exacerbates fibrosis

Given the observed reduction of miR-29a-3p in fibrosis models, we hypothesized that modulating miR-29a-3p levels could impact fibrosis outcomes. miR-29a-3p mimic treatment significantly reduced Scr and BUN levels compared to I/R + Vehicle and I/R + miR-29a-3p inhibitor groups (Fig. 4B, C). Histological analysis showed that the mimic treatment reduced the fibrotic area, FN, and α-SMA positive signals, while the inhibitor exacerbated

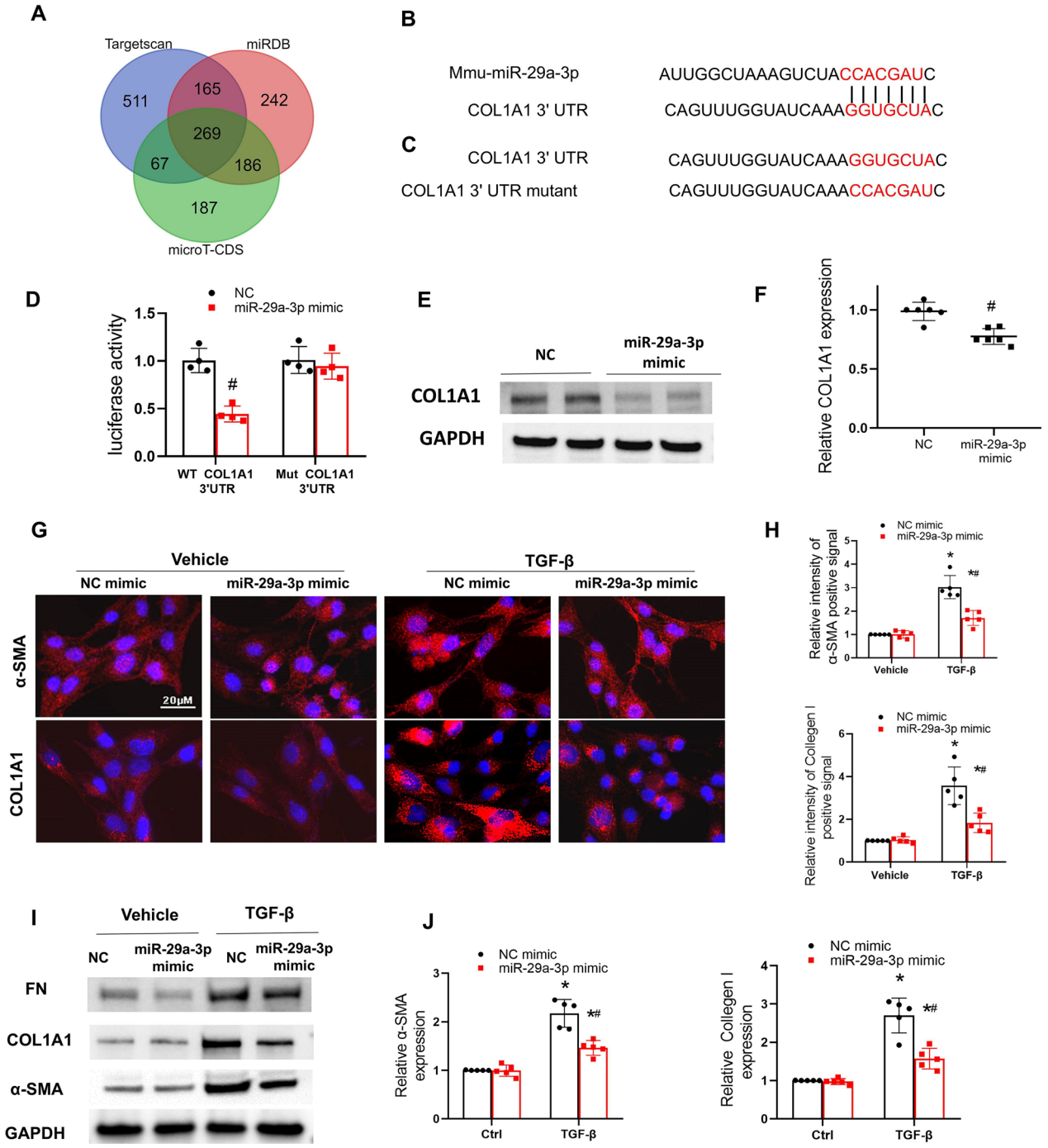

Fig. 6 (See legend on previous page.)

these markers (Fig. 4D, E). Western blot analysis confirmed these results, showing decreased levels of collagen I and α-SMA in the miR-29a-3p mimic group (Fig. 4F, G). These findings indicate that miR-29a-3p mimic alleviates, while its inhibitor worsens, I/R-induced renal fibrosis.

miR-29a-3p mimic reduces vascular rarefaction caused by I/R in mice, while miR-29a-3p inhibitor exacerbates it

To determine the specific effects of miR-29a-3p on vascular rarefaction post-I/R, we examined CD31 staining. The results showed that miR-29a-3p mimic increased the area of CD31-positive signals, whereas the inhibitor

exacerbated vascular rarefaction (Fig. 5A, B). Western blot analysis revealed that the mimic reduced ICAM-1, and VCAM-1 expression, while the inhibitor had the opposite effect (Fig. 5C, D). These results demonstrate that miR-29a-3p mimic protects against, and its inhibitor exacerbates, vascular rarefaction caused by I/R.

Collagen-1 is a target of miR-29a-3p in fibroblasts

To elucidate the molecular targets of miR-29a-3p in fibroblasts, we conducted sequence alignment and Luciferase Reporter Assays. These assays identified collagen I (COL1A1) as a direct target of miR-29a-3p (Fig. 6B, C). miR-29a-3p mimic significantly reduced COL1A1 protein levels in fibroblasts (Fig. 6E, F). Immunofluorescence and Western blot analyses confirmed that miR-29a-3p mimics decreased α-SMA and collagen I expression in fibroblasts treated with TGF-β (Fig. 6G–J). These findings suggest that miR-29a-3p regulates fibroblast activation by targeting collagen I.

miR-29a-3p mimics target TNFR1 in endothelial cells

Next, we explored the mechanisms by which miR-29a-3p exerts its protective effects in endothelial cells. Sequence alignment and luciferase reporter assays demonstrated that miR-29a-3p directly targets the 3' UTR of TNFRSF1A mRNA (Fig. 7A–C). miR-29a-3p mimics reduced TNFR1 protein levels in endothelial cells (Fig. 7D, E). Additionally, miR-29a-3p mimic treatment decreased the expression of ICAM-1 and VCAM-1 in endothelial cells treated with TNF-α (Fig. 7F, G). These results indicate that miR-29a-3p targets TNFR1 to exert its protective effects in endothelial cells.

Exosomes overexpressing miR-29a-3p are more effective than regular exosomes in protecting against renal fibrosis caused by I/R in mice

Finally, we compared the efficacy of exosomes overexpressing miR-29a-3p to regular exosomes in protecting against I/R-induced renal fibrosis. We performed PCR to detect the expression of miR-29a-3p in various organs, including the heart, spleen, lungs, and kidneys with or without exosomes treatment. The results showed a significant increase in miR-29a-3p levels specifically in the injured kidney, suggesting that the exosomes successfully homed to the site of injury (Fig. 8A). Exosomes overexpressing miR-29a-3p had higher levels of miR-29a-3p compared to regular exosomes (Fig. 8B). These exosomes provided superior protection, as evidenced by significantly lower Scr and BUN levels, reduced tubular injury scores, and decreased fibrosis and collagen I-positive areas compared to regular exosome treatment (Fig. 8C–F). Western blot analysis confirmed these protective effects, showing lower levels of TNFR1, ICAM-1, VCAM-1, collagen I, and α-SMA in the miR-29a-3p overexpressing exosome group (Fig. 8G–J). Overall, these findings highlight the enhanced therapeutic potential of exosomes overexpressing miR-29a in renal fibrosis.

Conclusion

In conclusion, our study demonstrates that exosomes derived from hucMSCs, especially those enriched with miR-29a-3p, effectively mitigate renal fibrosis and vascular rarefaction following I/R injury. miR-29a-3p targets COL1A1 in fibroblasts to reduce fibrosis and TNFR1 in endothelial cells to preserve vascular integrity. These findings highlight the therapeutic potential of miR-29a-3p-enriched exosomes in treating renal fibrosis and improving kidney function post-ischemia.

Discussion

Our study uncovered several critical findings that highlight the therapeutic potential of stem cell-derived exosomes in treating renal fibrosis. Firstly, exosome treatment significantly reduced post-ischemic fibrosis by acting on multiple cell types. Secondly, we observed that miR-29a-3p expression is reduced during renal fibrosis, whereas mesenchymal cell-derived exosomes are rich in

(See figure on next page.)

Fig. 7 miR-29a-3p Mimics Target TNFR1 in Endothelial Cells **A** Sequence alignment of miR-29a-3p with the 3'UTR of TNFRSF1A mRNA, highlighting the target binding site. **B** Sequence of the wild-type (WT) and mutant (Mut) TNFRSF1A 3'UTR used in luciferase reporter assays. **C** Luciferase activity assay showing the relative luciferase activity in cells transfected with WT or Mut TNFRSF1A 3'UTR constructs and miR-29a-3p mimics. Data are presented as mean ± SD (n = 3). #$p < 0.05$ vs. NC + WT TNFRSF1A 3'UTR. **D** Western blot analysis of TNFR1 and GAPDH in endothelial cells transfected with NC or miR-29a-3p mimics. **E** Quantification of TNFR1 protein expression normalized to GAPDH. Data are presented as mean ± SD (n = 6). #$p < 0.05$ vs. NC. **F** Representative immunofluorescence images of endothelial cells treated with vehicle or TNF-α and transfected with NC or miR-29a-3p mimics, stained for ICAM-1 and VCAM-1. Scale bars: 20 μm. **G** Quantification of the relative intensity of ICAM-1 and VCAM-1 positive staining in fibroblasts. Data are presented as mean ± SD (n = 5). *$p < 0.05$ vs. Vehicle + NC mimic, #$p < 0.05$ vs. TNF-α + NC mimic. #$p < 0.05$ vs. NC. **H** Western blot analysis of ICAM-1, VCAM-1, and GAPDH in endothelial cells treated with TNF-α and transfected with NC or miR-29a-3p mimics. **I** Quantification of ICAM-1 and VCAM-1 protein expression normalized to GAPDH. Data are presented as mean ± SD (n = 6). *$p < 0.05$ vs. Ctrl + NC, #$p < 0.05$ vs. TNF-α + NC

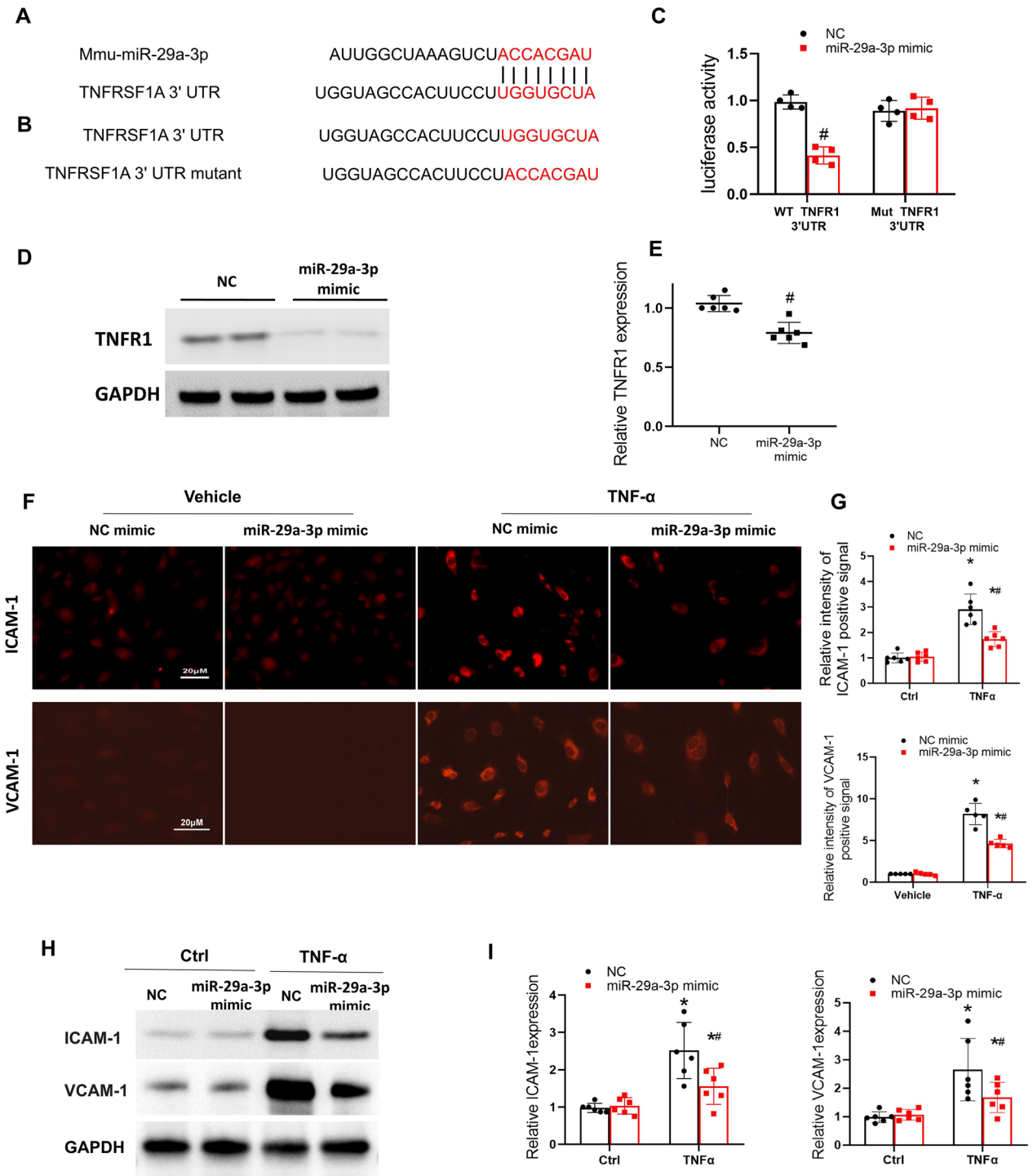

Fig. 7 (See legend on previous page.)

miR-29a-3p. Overexpressing miR-29a-3p in the kidney improved both renal function and the degree of fibrosis following ischemic injury. Thirdly, miR-29a-3p binds to the 3' UTRs of COL1A1 mRNA in fibroblasts, thereby decreasing the secretion of fibrotic factors, and targets TNFR1 in endothelial cells, reducing endothelial cell damage. Finally, exosomes overexpressing miR-29a-3p were found to more effectively alleviate I/R-induced fibrosis. These findings underscore the multifaceted therapeutic potential of miR-29a-3p-enriched exosomes in

mitigating renal fibrosis and enhancing kidney function post-ischemia.

The progression of CKD follows a common pathway where normal renal parenchyma is progressively replaced by matrix proteins such as collagen I, III, IV, and fibronectin [1]. Initially, the deposition of fibrotic matrix post-injury can aid the tissue repair process, and in cases of mild injury, it is subsequently resorbed during tissue remodeling [22]. Various cell types, including endothelial cells, renal tubular epithelial cells, and myofibroblasts, are involved in the progression of TIF. However, during chronic injury in CKD, the continuous deposition of fibrotic matrix disrupts the organ's architecture, reduces blood supply, and impairs its function. To address both acute injury and chronic fibrosis phases, we administered 50 μg of mesenchymal cell-derived exosomes overexpressing miR-29a-3p at −1 d, 0 d, 3 d, 6 d, and 9 d post-IRI. This multi-dose regimen, based on the long-term nature of fibrosis and findings from prior studies demonstrating dose-dependent exosome efficacy, showed significant therapeutic benefits. For example, Liu et al. [23] and Zeng et al. [24] reported optimal effects with doses of 100 μg in similar models. Our repeated dosing strategy was effective in improving fibrosis and vascular rarefaction without observable adverse effects, highlighting its potential advantages over single-dose protocols. These results suggest that multiple administrations may be crucial for sustained therapeutic outcomes in chronic conditions like fibrosis. Future studies could further refine dosing regimens and explore exosome biodistribution to enhance therapeutic efficacy.

Stem cells are promising for treating post-ischemic fibrosis due to their self-renewal capability, differentiation potential, and paracrine functions [25]. However, the mechanisms behind their effectiveness are not fully understood. Studies suggest that the therapeutic benefits of stem cells are likely due to their ability to modulate the local microenvironment rather than direct differentiation into target cells [25]. Our study showed that stem cell-derived exosomes improved renal fibrosis in mice post-I/R. Exosomes are small extracellular vesicles (40–100 nm) rich in proteins and RNAs, particularly miRNAs, which are key to their function. We found that miR-29a-3p is highly expressed in mesenchymal stem cell-derived exosomes, whereas its expression decreases in renal tissue following I/R injury. This led us to hypothesize that stem cells might exert their anti-fibrotic effects via exsosomal delivery of miR-29a-3p. HucMSCs exosomes improved renal function and reduced fibrosis after I/R injury, with miR-29a-3p being highly expressed in the exosomes. Further in vivo and in vitro experiments confirmed that miR-29a-3p is crucial for the therapeutic effects of stem cells. Injecting miR-29a-3p mimics into the kidney improved renal function and reduced fibrosis post-I/R, while miR-29a-3p inhibitors worsened these conditions. These findings suggest that miR-29a-3p has a protective effect against I/R-induced renal fibrosis.

The deposition of fibrotic matrix post-injury facilitates tissue repair and is subsequently reabsorbed during the remodeling phase in cases of mild injury. However, during chronic injury in CKD, this fibrotic matrix deposition continues unchecked, ultimately disrupting organ structure, reducing blood supply, and impairing function. Collagen I is the most abundant matrix protein in renal fibrosis, but other collagens, including types III, V, VI, VII, and XV, and adhesive glycoprotein fibronectin also accumulate [26]. Through luciferase reporter assays, we validated that the 3' UTRs of COL1A1 are direct targets of miR-29a-3p. miR-29a-3p inhibits COL1A1 synthesis, reducing ECM production and alleviating renal fibrosis caused by I/R injury. Renal I/R injury induces renal interstitial fibrosis [6]. Fibroblast activation, characterized by α-SMA expression and the production of large amounts of ECM components, is a hallmark of kidney fibrogenesis. In vitro, we established a TGF-β1-induced activation model of NRK-49F fibroblasts, which exhibited increased expression of α-SMA and COL1A1. miR-29a-3p mimics significantly reduced fibroblast proliferation and downregulated α-SMA and COL1A1 expression, demonstrating miR-29a-3p's involvement in TGF-β-induced fibrosis. By targeting COL1A1, miR-29a-3p reduces ECM production and inhibits the progression of renal interstitial fibrosis.

(See figure on next page.)

Fig. 8 Exosomes Overexpressing miR-29a-3p Are More Effective Than Regular Exosomes in Protecting Against Renal Fibrosis Caused by I/R in Mice **A** Relative expression of miR-29a-3p after administration of exosomes overexpressing miR-29a-3p in kidney, lung, heart and spleen. *$p < 0.05$ vs. Ctrl + Vehicle, #$p < 0.05$ vs. I/R + Vehicle. **B** Relative expression of miR-29a-3p in regular exosomes and exosomes overexpressing miR-29a-3p. **C** Serum creatinine (Scr) levels in different groups. **D** Blood urea nitrogen (BUN) levels in different groups. **E** Representative images of kidney sections stained with Hematoxylin and Eosin (HE), Sirius Red, collagen I, and ICAM-1. Scale bars: 100 μm. **F** Quantification of tubular injury scores, positive Sirius Red staining area, and positive collagen I staining area. **G** Western blot analysis of TNFR1, ICAM-1, VCAM-1, and GAPDH in kidney tissues from indicated groups. **H** Densitometric analysis of Western blot bands normalized to GAPDH. **I** Western blot analysis of collagen I, α-SMA, and GAPDH in kidney tissues from different groups. **J** Densitometric analysis of Western blot bands normalized to GAPDH. Data are presented as mean ± SD (n = 6). *$p < 0.05$ vs. Ctrl, #$p < 0.05$ vs. I/R + Vehicle, &$p < 0.05$ vs. I/R + Exosome

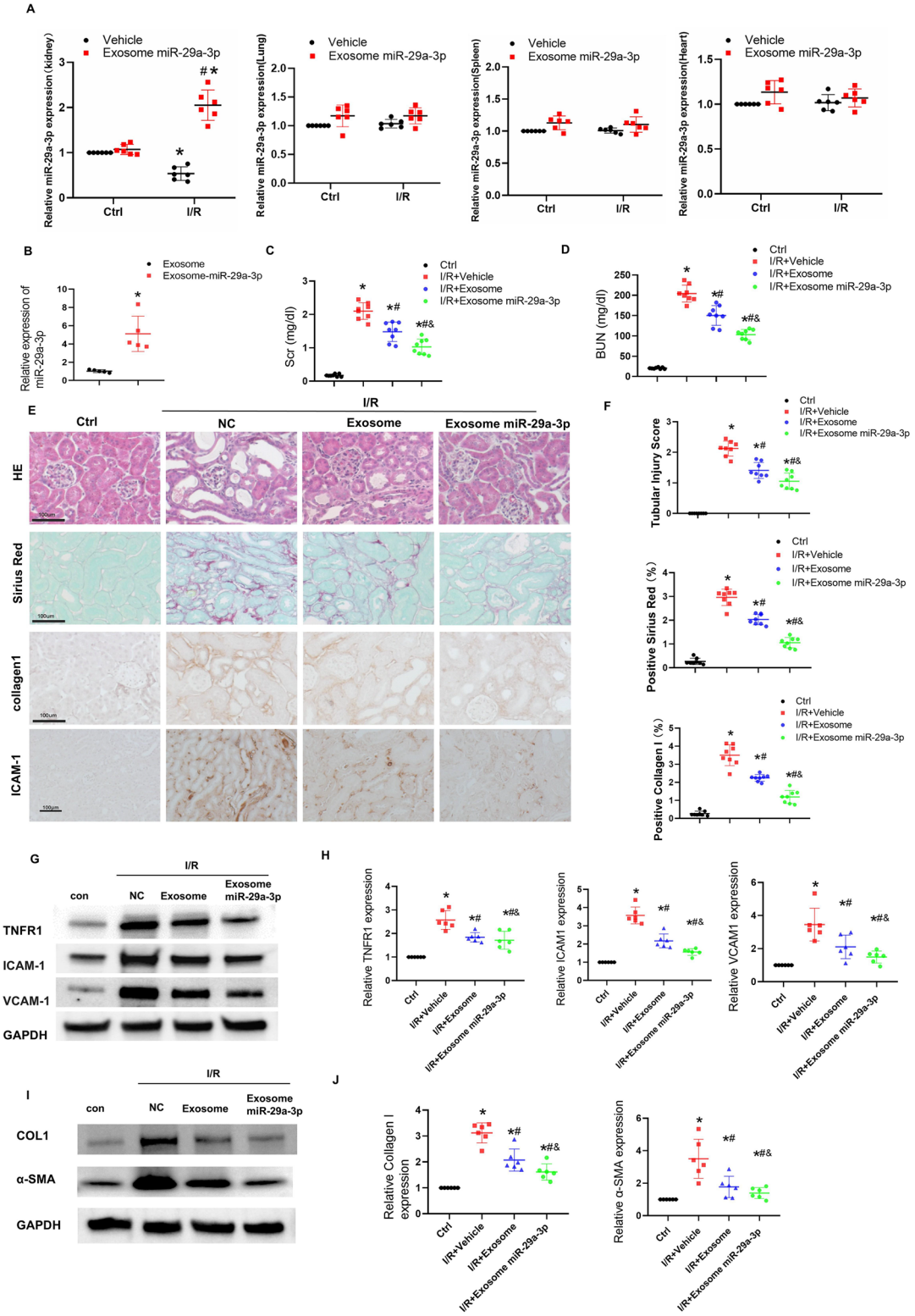

Fig. 8 (See legend on previous page.)

Damage to endothelial cells leading to microvascular rarefaction is a characteristic of CKD. Under the influence of inflammatory cytokines (such as interleukin-1β (IL-1β), interleukin-6 (IL-6), and TNF-α (tumor necrosis factor-α)), endothelial cells (ECs) undergo inflammatory activation, resulting in increased surface expression of cell adhesion molecules such as ICAM-1, VCAM-1, and E-selectin. TNFR1, encoded by the TNFRSF1A gene, is one of the primary TNF receptors [27]. TNFRSF1A is mainly expressed in endothelial cells in the kidney. TNFR1 induces various intracellular signaling pathways, including the nuclear factor-κB (NF-κB) and mitogen-activated protein kinase (MAPK) pathways. In our experiments, we found that TNFα significantly induces the expression of endothelial dysfunction biomarkers (VCAM-1, ICAM-1), providing direct evidence that TNFα plays a crucial role in endothelial dysfunction. Therefore, targeting the reduction of TNFR1 expression by transfecting miR-29a-3p mimic may be the reason for the protective effect of miR-29a-3p against TNFα-induced endothelial dysfunction, consistent with previous studies. Thus, the reduction of adhesion molecules caused by transfection with miR-29a-3p mimic indicates that miR-29a-3p plays a vital role in regulating endothelial dysfunction.

Although miRNAs also exist in the extracellular environment, miRNAs encapsulated in exosomes are protected from degradation and can more effectively target damaged sites to exert therapeutic effects [28]. It has been found that MSC-exo can localize to the injury sites after renal IRI and exert protective effects in a targeted manner [29]. We transfected stem cells with miR-29a-3p mimics, extracted the exosomes, and injected them into mice via the tail vein, which improved renal function and reduced renal fibrosis after I/R. In vivo experiments confirmed the protective effect of exosomal miR-29a-3p on renal fibrosis following I/R. Exosomes, which mediate cell–cell communication by delivering DNA, RNA, and proteins, are ideal drug delivery vehicles. First, unlike stem cells, they are safe and do not have tumorigenic potential. Second, MSC-derived non-immunogenic exosomes are well tolerated in vivo, have a longer circulation half-life, and lower immunogenicity compared to cells. Third, hucMSCs are a convenient and cost-effective source for drug delivery exosomes. Therefore, hucMSC-exos hold great promise as therapeutic agents. However, there are still obstacles to applying hucMSC-exos to POI therapy: there is an urgent need for scalable and cost-effective methods for the production and purification of exosomes, and further research is needed on the homing and immunomodulatory effects of hucMSC-exos.

In summary, our results demonstrate that mesenchymal cell-derived exosomes, particularly those overexpressing miR-29a-3p, have potent anti-fibrotic and vascular protective effects in renal fibrosis models. miR-29a-3p exerts its protective effects by targeting TNFR1 in endothelial cells and collagen I in fibroblasts, underscoring its therapeutic potential for renal fibrosis and vascular diseases.

Acknowledgements
We would like to thank Hamilton Company for providing the umbilical cord blood mesenchymal stem cells and RNA sequencing data of exosome. We used AI to polish the article language.

Author contributions
Jing Huang and Dingping Yang, Xiongfei Wu, Shangting Han contributed to the conception and design of the study. Yifei Yang, Fan Zhao, Rengui Chen, and Wenliang Liao were involved in data acquisition. Jiefu Zhu performed the analysis and interpretation of data. Jing Huang wrote the manuscript. Dingping Yang, Xiongfei Wu, and Shangting Han critically revised the manuscript. All authors read and approved the final manuscript.

Funding
This work was supported by the Knowledge Innovation Program of Wuhan-Shuguang Project (2023020201020505). The funding bodies had no role in the design of the study, collection, analysis, and interpretation of data, or in writing the manuscript.

Availability of data and materials
The datasets generated and/or analyzed during the current study are available from the corresponding author on reasonable request.

Declarations

Ethics approval and consent to participate
The study was approved by the Institutional Review Board of Renmin Hospital Wuhan Universtity. All procedures performed in studies involving animals were in accordance with the ethical standards of the institution and/or national research committee. The local ethics committee, adhering to the principles outlined in the Basel Declaration, approved the Program (Study of mechanisns associated with ischemia reperfusion injury in the kidney) design on March 9th, 2023 (Approval No. WDRM20230304B). The approved project titled "Collection of specimens from post-renal transplant and renal biopsy patients" was reviewed and approved by the Clinical Research Ethics Committee of Renmin Hospital, Wuhan University, for clinical research, under approval number WDRY2021-KS059 on November 30, 2021. All the patients provided written informed consent for participation in the study and the use of samples. HucMSCs, provided by Hamilton Biology, were derived from human umbilical cord tissue collected from a healthy donor with informed consent at Renmin Hospital. The collection and use of the umbilical cord tissue were approved by the Institutional Ethics Review Board of Renmin Hospital, Wuhan University [30].

Consent for publication
All authors confirm their consent for publication.

Competing interests
The authors declare that they have no competing interests.

Author details
[1]Department of Nephrology, Renmin Hospital of Wuhan University, Wuhan 430060, Hubei Province, China. [2]Department of Organ Transplantation, Renmin Hospital of Wuhan University, Wuhan 430060, Hubei Province, China. [3]Department of Nephrology, Guiqian International General Hospital, Guiyang, Guizhou, China. [4]Department of Nephrology, The First Hospital of Lanzhou University, Lanzhou 730000, China.

Received: 16 July 2024 Accepted: 11 February 2025
Published online: 12 March 2025

References

1. Gewin LS. Renal fibrosis: primacy of the proximal tubule. Matrix Biol. 2018;68–69:248–62.
2. Verissimo T, Faivre A, Rinaldi A, Lindenmeyer M, Delitsikou V, Veyrat-Durebex C, et al. Decreased renal gluconeogenesis is a hallmark of chronic kidney disease. J Am Soc Nephrol. 2022;33(4):810–27.
3. Lu YA, Liao CT, Raybould R, Talabani B, Grigorieva I, Szomolay B, et al. Single-nucleus RNA sequencing identifies new classes of proximal tubular epithelial cells in kidney fibrosis. J Am Soc Nephrol. 2021;32(10):2501–16.
4. McDaniels JM, Shetty AC, Kuscu C, Kuscu C, Bardhi E, Rousselle T, et al. Single nuclei transcriptomics delineates complex immune and kidney cell interactions contributing to kidney allograft fibrosis. Kidney Int. 2023;103(6):1077–92.
5. Huh SH, Ha L, Jang HS. Nephron progenitor maintenance is controlled through fibroblast growth factors and Sprouty1 interaction. J Am Soc Nephrol. 2020;31(11):2559–72.
6. Li L, Fu H, Liu Y. The fibrogenic niche in kidney fibrosis: components and mechanisms. Nat Rev Nephrol. 2022;18(9):545–57.
7. Chang FC, Liu CH, Luo AJ, Tao-Min Huang T, Tsai MH, Chen YJ, et al. Angiopoietin-2 inhibition attenuates kidney fibrosis by hindering chemokine C–C motif ligand 2 expression and apoptosis of endothelial cells. Kidney Int. 2022;102(4):780–97.
8. Yang B, Lan S, Dieudé M, Sabo-Vatasescu JP, Karakeussian-Rimbaud A, Turgeon J, et al. Caspase-3 is a pivotal regulator of microvascular rarefaction and renal fibrosis after ischemia-reperfusion injury. J Am Soc Nephrol. 2018;29(7):1900–16.
9. Ren J, Liu K, Wu B, Lu X, Sun L, Privratsky JR, et al. Divergent actions of renal tubular and endothelial type 1 IL-1 receptor signaling in toxin-induced AKI. J Am Soc Nephrol. 2023;34(10):1629–46.
10. Li Y, Liu P, Zhou Y, Maekawa H, Silva JB, Ansari MJ, et al. Activation of angiopoietin-Tie2 signaling protects the kidney from ischemic injury by modulation of endothelial-specific pathways. J Am Soc Nephrol. 2023;34(6):969–87.
11. Xu-Dubois YC, Ahmadpoor P, Brocheriou I, Louis K, Arzouk Snanoudj N, Rouvier P, et al. Microvasculature partial endothelial mesenchymal transition in early posttransplant biopsy with acute tubular necrosis identifies poor recovery renal allografts. Am J Transplant. 2020;20(9):2400–12.
12. Hasegawa K, Sakamaki Y, Tamaki M, Wakino S. PCK1 protects against mitoribosomal defects in diabetic nephropathy in mouse models. J Am Soc Nephrol. 2023;34(8):1343–65.
13. Liu B, Wei Y, He J, Feng B, Chen Y, Guo R, et al. Human umbilical cord-derived mesenchymal stromal cells improve myocardial fibrosis and restore miRNA-133a expression in diabetic cardiomyopathy. Stem Cell Res Ther. 2024;15(1):120.
14. Blijdorp CJ, Burger D, Llorente A, Martens-Uzunova ES, Erdbrügger U. Extracellular vesicles as novel players in kidney disease. J Am Soc Nephrol. 2022;33(3):467–71.
15. Sang X, Tang L, Zhao L, Xu N, Liu F, Shen Y, et al. Umbilical cord mesenchymal stem cell-derived exosomes promote axon regeneration during optic nerve injury through microRNA-dependent mTORC1 signalling. Clin Transl Med. 2023;13(7):e1319.
16. Muskan M, Abeysinghe P, Cecchin R, Branscome H, Morris KV, Kashanchi F. Therapeutic potential of RNA-enriched extracellular vesicles: the next generation in RNA delivery via biogenic nanoparticles. Mol Ther. 2024;32:2939–49.
17. Dalgaard LT, Sørensen AE, Hardikar AA, Joglekar MV. The microRNA-29 family: role in metabolism and metabolic disease. Am J Physiol Cell Physiol. 2022;323(2):C367–77.
18. Shi L, Zha H, Pan Z, Wang J, Xia Y, Li H, et al. DUSP1 protects against ischemic acute kidney injury through stabilizing mtDNA via interaction with JNK. Cell Death Dis. 2023;14(11):724.
19. Shi L, Song Z, Li Y, Huang J, Zhao F, Luo Y, et al. MiR-20a-5p alleviates kidney ischemia/reperfusion injury by targeting ACSL4-dependent ferroptosis. Am J Transplant. 2023;23(1):11–25.
20. Zhu J, Xiang X, Hu X, Li C, Song Z, Dong Z. miR-147 represses NDUFA4, inducing mitochondrial dysfunction and tubular damage in cold storage kidney transplantation. J Am Soc Nephrol. 2023;34(8):1381–97.
21. Song Z, Xia Y, Shi L, Zha H, Huang J, Xiang X, et al. Inhibition of Drp1-Fis1 interaction alleviates aberrant mitochondrial fragmentation and acute kidney injury. Cell Mol Biol Lett. 2024;29(1):31.
22. Humphreys BD. Mechanisms of renal fibrosis. Annu Rev Physiol. 2018;80:309–26.
23. Cao JY, Wang B, Tang TT, Wen Y, Li ZL, Feng ST, et al. Exosomal miR-125b-5p deriving from mesenchymal stem cells promotes tubular repair by suppression of p53 in ischemic acute kidney injury. Theranostics. 2021;11(11):5248–66.
24. Zhu F, Chong Lee Shin OLS, Pei G, Hu Z, Yang J, Zhu H, et al. Adipose-derived mesenchymal stem cells employed exosomes to attenuate AKI-CKD transition through tubular epithelial cell dependent Sox9 activation. Oncotarget. 2017;8(41):70707–26.
25. Hoang DM, Pham PT, Bach TQ, Ngo ATL, Nguyen QT, Phan TTK, et al. Stem cell-based therapy for human diseases. Signal Transduct Target Ther. 2022;7(1):272.
26. Genovese F, Manresa AA, Leeming DJ, Karsdal MA, Boor P. The extracellular matrix in the kidney: a source of novel non-invasive biomarkers of kidney fibrosis? Fibrogenesis Tissue Repair. 2014;7(1):4.
27. Kong DH, Kim YK, Kim MR, Jang JH, Lee S. Emerging roles of vascular cell adhesion molecule-1 (VCAM-1) in immunological disorders and cancer. Int J Mol Sci. 2018;19(4):1057.
28. Xu Y, Hu Y, Xu S, Liu F, Gao Y. Exosomal microRNAs as potential biomarkers and therapeutic agents for acute ischemic stroke: new expectations. Front Neurol. 2021;12:747380.
29. Tang TT, Wang B, Li ZL, Wen Y, Feng ST, Wu M, et al. Kim-1 targeted extracellular vesicles: a new therapeutic platform for RNAi to treat AKI. J Am Soc Nephrol. 2021;32(10):2467–83.
30. Zhang Y, Le X, Zheng S, Zhang K, He J, Liu M, et al. MicroRNA-146a-5p-modified human umbilical cord mesenchymal stem cells enhance protection against diabetic nephropathy in rats through facilitating M2 macrophage polarization. Stem Cell Res Ther. 2022;13(1):171.

Publisher's Note